This article was downloaded by:
On: *21 January 2011*
Access details: *Access Details: Free Access*
Publisher *Taylor & Francis*
Informa Ltd Registered in England and Wales Registered Number: 1072954 Registered office: Mortimer House, 37-41 Mortimer Street, London W1T 3JH, UK

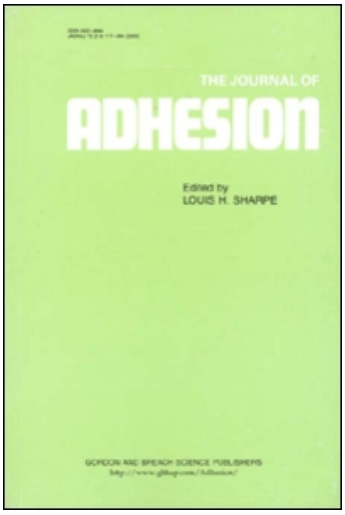

The Journal of Adhesion
Publication details, including instructions for authors and subscription information:
http://www.informaworld.com/smpp/title~content=t713453635

Delamination Mechanics of a Clamped Rectangular Membrane in the Presence of Long-Range Intersurface Forces: Transition from JKR to DMT Limits

Guangxu Li[a]; Kai-Tak Wan[a]
[a] Mechanical and Industrial Engineering, Northeastern University, Boston, MA, USA

Online publication date: 12 March 2010

To cite this Article Li, Guangxu and Wan, Kai-Tak(2010) 'Delamination Mechanics of a Clamped Rectangular Membrane in the Presence of Long-Range Intersurface Forces: Transition from JKR to DMT Limits', The Journal of Adhesion, 86: 3, 335 — 351
To link to this Article: DOI: 10.1080/00218460903482531
URL: http://dx.doi.org/10.1080/00218460903482531

PLEASE SCROLL DOWN FOR ARTICLE

Full terms and conditions of use: http://www.informaworld.com/terms-and-conditions-of-access.pdf

This article may be used for research, teaching and private study purposes. Any substantial or systematic reproduction, re-distribution, re-selling, loan or sub-licensing, systematic supply or distribution in any form to anyone is expressly forbidden.

The publisher does not give any warranty express or implied or make any representation that the contents will be complete or accurate or up to date. The accuracy of any instructions, formulae and drug doses should be independently verified with primary sources. The publisher shall not be liable for any loss, actions, claims, proceedings, demand or costs or damages whatsoever or howsoever caused arising directly or indirectly in connection with or arising out of the use of this material.

The Journal of Adhesion, 86:335–351, 2010
Copyright © Taylor & Francis Group, LLC
ISSN: 0021-8464 print/1545-5823 online
DOI: 10.1080/00218460903482531

Taylor & Francis
Taylor & Francis Group

Delamination Mechanics of a Clamped Rectangular Membrane in the Presence of Long-Range Intersurface Forces: Transition from JKR to DMT Limits

Guangxu Li and Kai-Tak Wan
Mechanical and Industrial Engineering, Northeastern University, Boston, MA, USA

A 1-dimensional rectangular freestanding membrane clamped at opposite ends adheres to the planar surface of a rectangular punch. A tensile load applied to the punch causes the membrane to deform and gradually delaminate from the substrate. At equilibrium, the applied load is balanced by the disjoining pressure at the membrane-punch interface with range, y*, and magnitude,* p*. Applying the Dugdale-Barenblatt-Maugis cohesive zone approximation, the disjoining pressure is taken to be uniform and confined to a finite cohesive length at the contact edge. For a fixed adhesion energy,* $\gamma = \mathrm{p}\,\mathrm{y}$*, we investigate the following: (i) the Derjaguin-Muller-Toporov (DMT) limit where* $\mathrm{y} \to \infty$ *and* $\mathrm{p} \to 0$*, (ii) the Johnson-Kendall-Roberts (JKR) limit where* $\mathrm{y} \to 0$ *and* $\mathrm{p} \to \infty$*, and (iii) the general case for intermediate but finite* y *and* p*. Delamination continues until the contact area shrinks to a line prior to "pinch-off". The results are compared with the 2-dimensional axisymmetric membrane counterpart.*

Keywords: Adhesion; Cohesive zone; Delamination; Disjoining pressure; Pinch-off

Downloaded At: 19:39 21 January 2011

1. INTRODUCTION

Interfacial adhesion has significant impacts in nano-technology [1] and life sciences [2]. Historically, the classical Hertz contact theory [3] is widely adopted to account for mechanical contact between two spheres or a sphere on planar substrate. It was Derjaguin [4] who pioneered in incorporating long-range intersurface forces into solid–solid adhesion interfaces that led to the Derjaguin-Muller-Toporov (DMT) model [5].

Received 6 May 2009; in final form 6 October 2009.

Address correspondence to Kai-Tak Wan, Northeastern University, Mechanical and Industrial Engineering, 334 Snell Engineering Center, 360 Huntington Avenue, Boston, MA 02115, USA. E-mail: ktwan@coe.neu.edu

Johnson *et al.* [6] further considered the local elastic deformation of the adhering solids in the presence of short-range (or zero range) interactions and perfected the adhesion theory of Johnson-Kendall-Roberts (JKR). Maugis later adopted the Dugdule-Barenblatt-Maugis cohesive zone approximation to model finite range and magnitude of intersurface forces, and derived the transition from JKR to DMT limits [7]. Notwithstanding the many colossal applications and rich physical insights of these celebrated models, they are inadequate to account for membrane adhesion. When clamped membranes or membranous vesicles come into contact with an adhering substrate, they conform to the substrate geometry and undergo bending or stretching, rather than developing the standard Hertz compression within the contact area. The strain field and the resulting interfacial adhesion mechanics are, therefore, distinctly different from the classical Hertz contact and the associated adhesion models. This is particularly true in the context of biological cells, biomimetic microcapsules [8], micro-electromechanical systems (MEMS) with moveable bridges and diaphragms [9], gecko feet [10], carbon nano-tubes [11], and long range interaction between thin curved shells and wavy substrates [12].

Downloaded At: 19:39 21 January 2011

Recently, we constructed adhesion models for the limiting case of zero-range intersurface forces (JKR-limit) and applied the model to (a) a 1-D rectangular membrane clamped at the opposite ends and (b) a 2-D axisymmetric membrane clamped at the circular periphery, where sample membranes are allowed to deform by mixed bending-stretching with or without residual stress [13–16]. We further relaxed the JKR-DMT constraint to allow intermediate magnitude and range of intersurface forces and refined the 2-D circular membrane adhesion mechanics [17]. This paper is a further extension to a 1-D rectangular membrane. Despite the similar configurations, the new 1-D model possesses characteristic behavior contrasting the 2-D counterpart.

In our previous work [16], the solution is derived for a similar loading configuration: a thin film clamped at the opposite ends deforms under pure plate bending and in the presence of a fixed tensile residual stress. Interfacial adhesion considered is limited to zero surface force range, *i.e.*, JKR limit. In this paper, we consider the membrane to be under pure stretching such that membrane stress varies as the external load increases, and a long range surface force.

2. THEORY

Figure 1a shows a rectangular membrane of unit width being clamped at the opposite ends and adhered to the planar surface of a flat punch with the same length and width. Upon an external tensile load applied

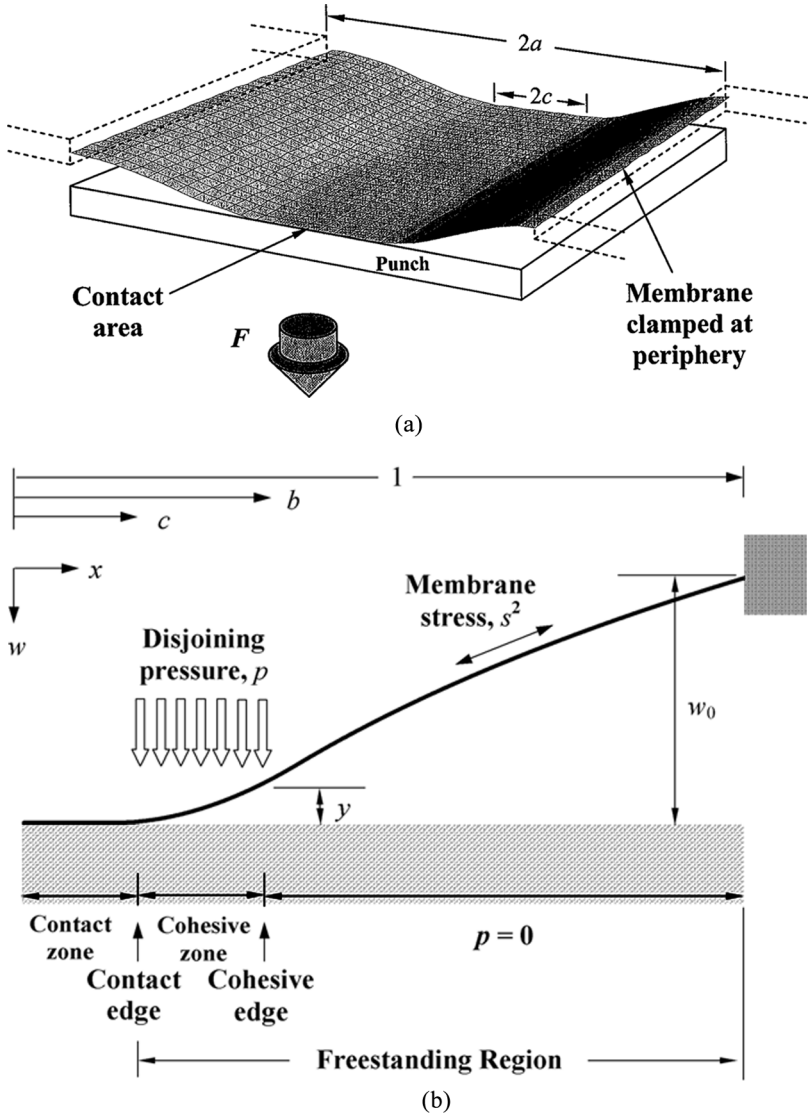

FIGURE 1 (a) Schematic of a clamped rectangular membrane adhered to a planar punch surface. (b) Drawing in normalized coordinates and variables.

to the punch, delamination occurs reducing the contact area. Figure 1b shows a schematic of half the membrane profile, $w(x)$, from the centerline to the clamped edge, $0 \leq x \leq 1$. All variables and their

Downloaded At: 19:39 21 January 2011

dimensionless equivalences are defined and listed in Table 1. All horizontal dimensions are scaled by the membrane half length, $\boldsymbol{a}$, while vertical dimensions are scaled by the membrane thickness, $\boldsymbol{h}$. The long-range intersurface force or disjoining pressure, p, acting across the membrane-substrate gap gives rise to a cohesive zone immediately behind the delamination front ($x = c$). The cohesive edge ($x = b$) divides the freestanding membrane into an inner cohesive zone where p acts ($c \le x \le b$) and a traction free outer region ($b \le x \le 1$). A few basic assumptions are taken to construct the new adhesion model: (i) the membrane is deformed by membrane-stretching only with negligible plate-bending (*i.e.*, zero flexural rigidity), (ii) the debonding angle, θ, is small with $d\boldsymbol{w}/d\boldsymbol{x} = \tan\theta \approx \sin\theta \approx 0$, and (iii) any residual stress and sliding in the contact region are ignored [18].

2.1. The Attractive Surface Force Law

The form of exact disjoining pressure is mathematically involved [19], though the net effect is here taken to be attractive in the present context. A finite magnitude, p, and a finite range, y, according to the

Downloaded At: 19:39 21 January 2011

TABLE 1 Normalized Coordinates and Variables

	Physical parameters (bold)	Normalized parameters
Geometrical parameters	$\boldsymbol{x}$ = horizontal distance (m) $\boldsymbol{w}$ = deformation profile (m) $\boldsymbol{w_0}$ = vertical displacement of punch (m) $\boldsymbol{a}$ = half width of sample membrane (m) $\boldsymbol{c}$ = half width of contact area (m) $\boldsymbol{b}$ = half width of cohesive edge (m) $\boldsymbol{h}$ = membrane thickness (m)	$x = \dfrac{\boldsymbol{x}}{\boldsymbol{a}}$, $w = \dfrac{\boldsymbol{w}}{\boldsymbol{h}}$, $\quad w_0 = \dfrac{\boldsymbol{w}_0}{\boldsymbol{h}}$, $c = \dfrac{\boldsymbol{c}}{\boldsymbol{a}}$, $\quad b = \dfrac{\boldsymbol{b}}{\boldsymbol{a}}$
Material parameters	$\boldsymbol{\nu}$ = Poisson's ratio $\boldsymbol{E}$ = elastic modulus (Nm^{-2}) $\boldsymbol{\sigma}$ = tensile membrane stress (Nm^{-2}) $\boldsymbol{\gamma}$ = interfacial adhesion energy (Jm^{-2}) $\boldsymbol{p}$ = disjoining pressure (Nm^{-2}) $\boldsymbol{y}$ = surface force range (m)	$s = \boldsymbol{\sigma}^{1/2}\left[\dfrac{12(1-\boldsymbol{\nu}^2)\boldsymbol{a}^2}{\boldsymbol{Eh}^2}\right]^{1/2}$ $\gamma = \boldsymbol{\gamma}\left[\dfrac{12(1-\boldsymbol{\nu}^2)\boldsymbol{a}^4}{\boldsymbol{Eh}^5}\right]$ $p = \boldsymbol{p}\left[\dfrac{12(1-\boldsymbol{\nu}^2)\boldsymbol{a}^4}{\boldsymbol{Eh}^4}\right]$ $y = \dfrac{\boldsymbol{y}}{\boldsymbol{h}}$
Mechanical loading	$\boldsymbol{F}$ = applied external force (N) $\boldsymbol{U}$ = energy terms (J)	$F = \boldsymbol{F}\left[\dfrac{12(1-\boldsymbol{\nu}^2)\boldsymbol{a}^3}{\boldsymbol{Eh}^4}\right]$ $U = \boldsymbol{U}\left[\dfrac{12(1-\boldsymbol{\nu}^2)\boldsymbol{a}^3}{\boldsymbol{Eh}^5}\right]$

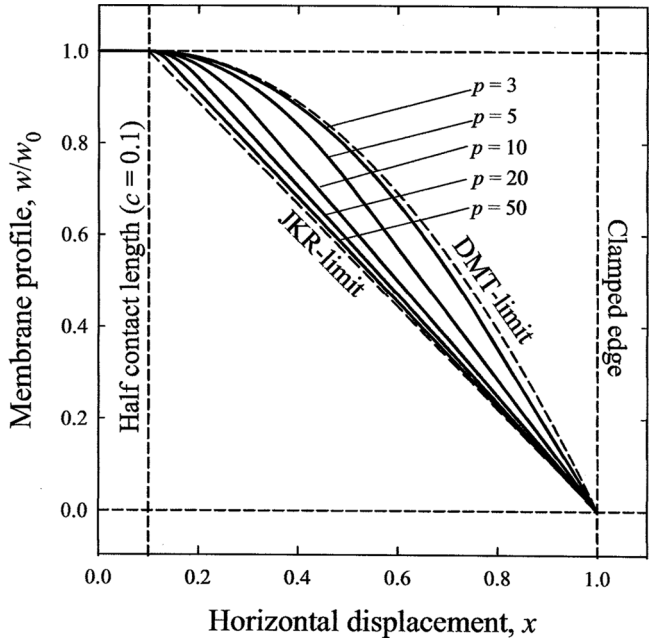

FIGURE 2 Membrane profile for fixed half contact length $c = 0.1$ and a range of disjoining pressure.

Downloaded At: 19:39 21 January 2011

Dugdale-Barenblatt-Maugis model [20,21], are assumed such that

$$\begin{aligned}\Phi(w) &= p \quad \text{within the cohesive zone}, c < x \le b \text{ and } 0 < (w_0 - w) \le y \\ &= 0 \quad \text{without the cohesive zone}, b < x \le 1 \text{ and } y < (w_0 - w) \le w_0.\end{aligned} \tag{1}$$

The JKR limit corresponds to $y \to 0$, $p \to \infty$, and $b \to c$, and the DMT limit $y \to \infty$, $p \to 0$, and $b \to 1$. The interfacial adhesion energy, $\gamma = p\,y$, is a material parameter. Mechanical equilibrium requires $F = 2p\,(b–c)$. Upon loading, a small punch displacement with $w_0 \le y$ requires the cohesive zone to extend to the clamped edge ($x = 1$), alluding to a *pseudo* DMT limit. Large displacement with $w_0 > y$ causes the cohesive edge to retract from the edge and give rise to a fully developed cohesive zone entirely confined to the freestanding region.

2.2. Membrane Profile

The external load applied to the punch is balanced by the disjoining pressure, resulting in a deformed membrane profile governed by

$$\begin{cases} -\boldsymbol{\sigma h}\cdot\nabla^2\boldsymbol{w}=\boldsymbol{p} & \text{for } \boldsymbol{c}<\boldsymbol{x}\le\boldsymbol{b} \\ -\boldsymbol{\sigma h}\cdot\nabla^2\boldsymbol{w}=(\boldsymbol{F}/2)\cdot\delta(\boldsymbol{x}) & \text{for } \boldsymbol{b}<\boldsymbol{x}\le\boldsymbol{a}, \end{cases} \tag{2}$$

where $\nabla^2 = d^2/d\boldsymbol{x}^2$ is the Laplacian operator and $\delta(\boldsymbol{x})$ is the Dirac's delta function denoting the applied load at the centerline ($x=0$). Equation (2) can be rewritten as

$$\begin{cases} -s^2\cdot\frac{dw}{dx}=p\cdot x & \text{for } c<x\le b \\ -s^2\cdot\frac{dw}{dx}=p(b-c) & \text{for } b<x\le 1, \end{cases} \tag{3}$$

which can be solved exactly to yield

$$w=\begin{cases} \frac{p}{2s^2}(-x^2+2cx+2b-b^2-2c) & \text{for } c<x\le b \\ \frac{p(b-c)}{s^2}(-x+1) & \text{for } b<x\le 1. \end{cases} \tag{4}$$

Figure 2 shows typical profiles for $c=0.1$ and a range of p. Note the "cusp"-like geometry in the cohesive zone leading to the contact edge in reminiscence of Barenblatt's crack [20–22], and the linear profile in the traction-free region alluding to the Griffith's parabolic geometry [23]. In the limit of $p\to\infty$ and $b\to c$, the cusp vanishes and the freestanding region is linear throughout. The punch displacement is given by

$$w_0 = w(x=c) = -\frac{p}{2s^2}(b+c-2)(b-c) \tag{5}$$

and the surface force range

$$y = w_0 - w(x=b). \tag{6}$$

2.3. Energy Balance

Total energy of the membrane-substrate system is given by $U_T = U_E - U_S$, with U_E the elastic energy due to membrane stretching and U_S the surface energy to create new surfaces. For delamination to occur, $(\partial U_T/\partial c)_{w_0=\text{constant}} = 0$. Since the mechanical response of a thin flexible membrane is always cubic with $F\propto w_0^3$, $U_E = \int F\cdot dw_0 = 1/4\ F\cdot w_0$. Alternatively, the energy density of $s^4/24$ leads to $U_E =$ energy density $\times$ area. The average membrane stress is given by

$$s^2=\begin{cases} \frac{12}{b-c}\int_c^b \frac{1}{2}\left(\frac{dw}{dx}\right)^2 dx & \text{for } c<x\le b \\ \frac{12}{1-b}\int_b^1 \frac{1}{2}\left(\frac{dw}{dx}\right)^2 dx & \text{for } b<x\le 1. \end{cases} \tag{7}$$

Downloaded At: 19:39 21 January 2011

Substituting w in Eqs. (4) into (7),

$$s = \begin{cases} 2^{1/6}(b-c)^{1/3}p^{1/3} & \text{for } c < x \le b \\ 6^{1/6}(b-c)^{1/3}p^{1/3} & \text{for } b < x \le 1. \end{cases} \tag{8}$$

It is noted that s carries now a slightly different definition. Rather than being a function of x, it is a constant depending on the disjoining pressure and cohesive zone length. In other words, s cannot be substituted back to Eq. (4) to yield the membrane profile. The sole purpose of averaging membrane stress is to yield an analytical expression for energy. The elastic energy is, therefore, given by

$$U_E = \underbrace{\frac{s^4}{24} \cdot 2 \cdot (b-c)}_{\text{for } c<x\le b} + \underbrace{\frac{s^4}{24} \cdot 2 \cdot (1-b)}_{\text{for } b<x\le 1}. \tag{9}$$

Substituting s in Eqs. (6) and (8) into (9),

$$U_E = \frac{16}{3(b-c)^3}y^4 + \frac{3}{(1-b)^3}(w_0 - y)^4. \tag{10}$$

The surface energy per unit area has a maximum in the contact zone with $U_S = \gamma$ $(2c)$, decreases in the cohesive zone, and reaches zero at the cohesive edge. Therefore,

$$U_S = 2c \cdot \gamma + 2\int_c^b p \cdot [y - (w_0 - w)] \cdot dx. \tag{11}$$

Substituting Eqs. (4), (5), and (6) into (11),

$$U_S = 2c \cdot \gamma - (b-c) \cdot \left\{ \left(\frac{2}{3} \cdot \frac{b-c}{2-b-c} \right) p w_0 - 2\gamma \right\}. \tag{12}$$

2.4. The JKR Limit

In the JKR limit, $y \to 0$, $p \to \infty$, and $b \to c$. The disjoining pressure turns into a Dirac's delta function at the contact edge, the cohesive zone width (b–c) reduces to zero, and the traction-free freestanding membrane becomes linear, and is given by

$$w = w_0 \left(\frac{1-x}{1-c} \right) \quad \text{with} \quad w_0 = \frac{F}{2s^2}(1-c). \tag{13}$$

The mechanical response *without* delamination is found to be

$$F = \frac{12 w_0^3}{(1-c)^3} \tag{14}$$

Downloaded At: 19:39 21 January 2011

which is cubic for fixed c. The energy terms reduce to

$$U_E = \frac{3w_0^4}{(1-c)^3} \quad \text{and} \quad U_S = 2c \cdot \gamma. \tag{15}$$

An energy balance yields the delamination trajectory,

$$w_0 = \frac{2^{1/4}}{3^{1/2}}(1-c)\gamma^{1/4} \quad \text{and} \quad F = 4\left(\frac{2^{3/4}}{3^{1/2}}\right)\gamma^{3/4}. \tag{16}$$

Equations (13) to (16) are consistent with our earlier results [14]. Figure 3 shows $F(w_0)$ in the JKR limit. As F increases from null, the contact area remains intact until F reaches a maximum at $F_{\max} = (4 \times 2^{3/4}/3^{1/2})\gamma^{3/4} \approx 3.884\gamma^{3/4}$ (N.B. $F_{max} = 4\gamma^{3/4}$ in Figure 3 for reasons discussed later), which is consistent with our earlier result [14]. In a displacement control configuration, further increase in w_0 leads

Downloaded At: 19:39 21 January 2011

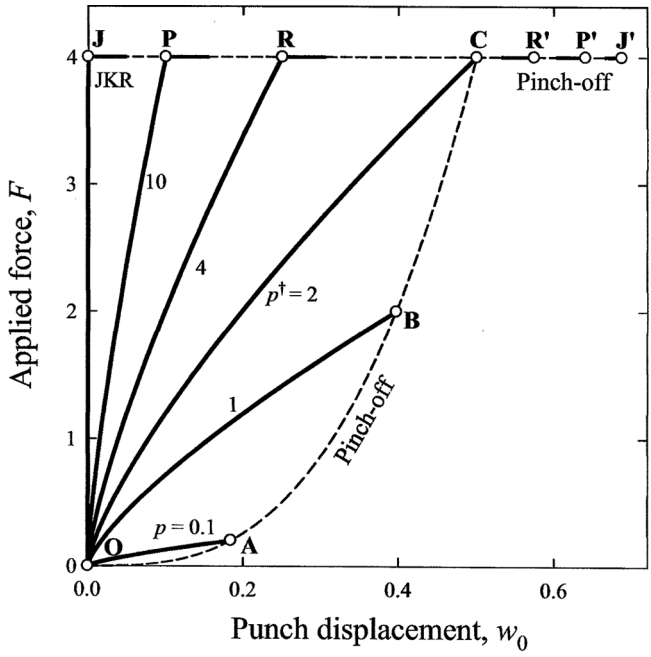

FIGURE 3 Mechanical response for a range of disjoining pressure. The dashed curve OABC corresponds to pinch-off with line contact of the DMT limit. Pinch-off occurs at R′, P′, and J′ for $p = 4$, 10, and JKR limit, respectively.

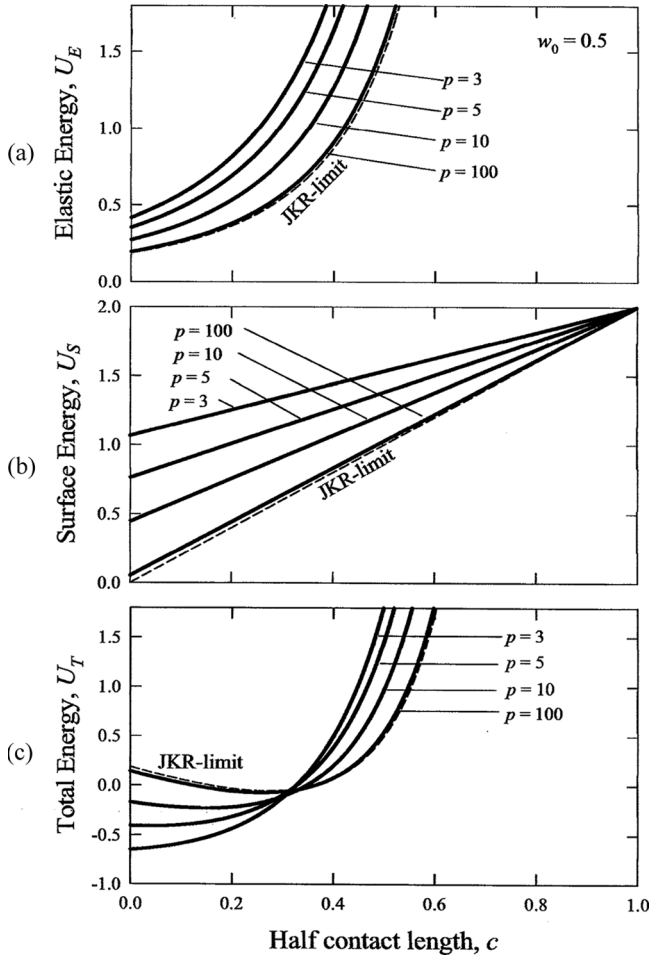

FIGURE 4 Energy as a function of contact length for punch displacement $w_0 = 0.5$ and a range of disjoining pressure: (a) elastic energy stored in the membrane, (b) surface energy, and (c) total energy of the membrane-punch system. The dashed curve is the JKR limit.

to a steady delamination along JJ′ at constant F_{max} under neutral equilibrium. At J′, the contact area reduces to a central line contact ($c = 0$). An incremental increase in w_0 requires the membrane to snap from the substrate or "pinch-off" at $w_0^* = (2^{1/4}/3^{1/2})\gamma^{1/4} \approx 0.6866\gamma^{1/4}$. Since the membrane-punch gap now exceeds the disjoining pressure range ($w_0 > y$) herein, the membrane no longer senses the presence of the substrate and, thus, returns to its non-deformed plane.

Downloaded At: 19:39 21 January 2011

2.5. The DMT Limit

In the neo-DMT limit, $y \to \infty$, $p \to 0$, and $b \to 1$. Here we consider a pseudo-DMT limit (abbreviated as DMT limit hereafter) where $b = 1$, but p does not necessarily vanish and $y \geq w_0$. The cohesive zone is underdeveloped, and the disjoining pressure is present in the entire non-contact freestanding region. The cusp-like membrane profile is found from Eq. (4) to be

$$w = w_0\left(\frac{-x^2 + 2cx - 2c + 1}{c^2 - 2c + 1}\right) \quad \text{with} \quad w_0 = \frac{p}{2s^2}(c^2 - 2c + 1). \tag{17}$$

The constitutive relation without delamination is, therefore,

$$F = \frac{32w_0^3}{(1-c)^3}. \tag{18}$$

The energy terms become

$$U_E = \frac{16w_0^4}{3(1-c)^3} \quad \text{and} \quad U_S = 2\gamma - \frac{2}{3}pw_0(1-c). \tag{19}$$

Energy balance requires

$$w_0 = \left(\frac{p}{16}\right)^{1/3}(1-c)^{4/3} \quad \text{and} \quad F = 4p^{3/4}w_0^{3/4}. \tag{20}$$

Figure 5 shows $F(w_0)$ for $p = 0.1$. At O ($F = 0$, $w_0 = 0$), the membrane is in full contact with the punch. As delamination proceeds along path OA, F monotonically increases while the contact area shrinks. At A, the contact area reduces to a line with $c = 0$. Further increase in w_0 causes the membrane to pinch-off. Regardless of the surface force range, the initial loading ($w_0 = 0$ and $y > w_0$) always begins with the DMT limit. The pinch-off locus, hereafter denoted by the asterisk, can be obtained by putting $c \to 0$ into Eq. (18), yielding $F^* = 32(w_0^*)^3$. The condition $w_0^* \leq y$ implies that the punch displacement falls short of the surface force range when the membrane completely separates from the punch. In order words, the membrane can still sense the presence of the punch and remains deformed until $w_0 > y$. The special case of $w_0^* = y$ denoted by the dagger superscript requires $b = 1$ and $p^\dagger = 16(y^\dagger)^3$, which is consistent with our earlier result [9]. Now $\gamma = p^\dagger y^\dagger = 1$, $p = p^\dagger = 16^{1/4} = 2$, which is the maximum possible disjoining pressure for the DMT limit to remain valid, and $y^\dagger = 0.5$. The two limits according to JKR and DMT present distinctly different delamination processes.

Downloaded At: 19:39 21 January 2011

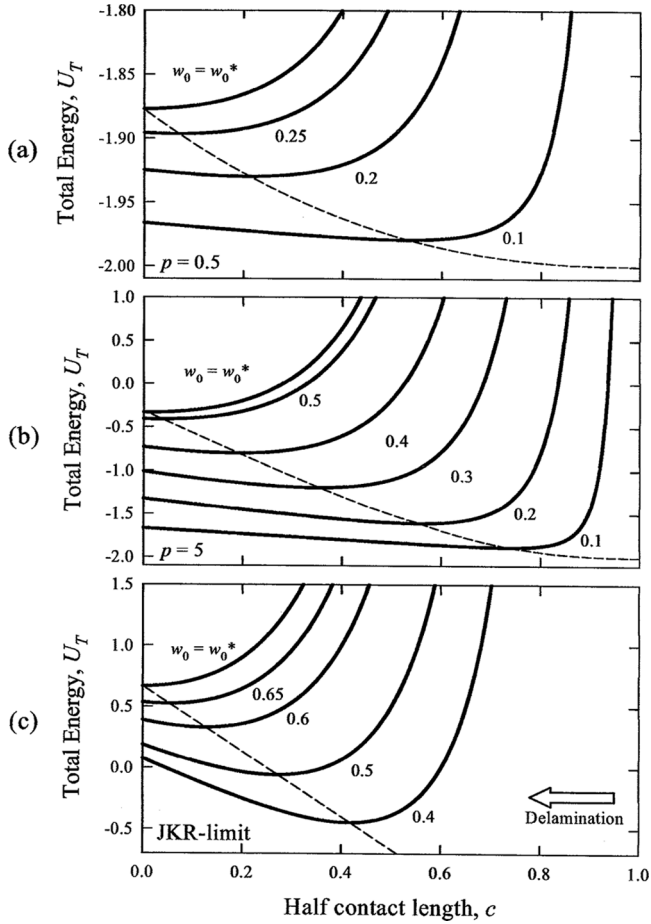

FIGURE 5 Total energy of the membrane-punch system for disjoining pressure (a) $p = 0.5$, (b) $p = 5$, and (c) $p \to \infty$ (JKR limit).

2.6. The DMT-JKR Transition

For disjoining pressure with intermediate range and magnitude, a Mathematica code is developed for fixed w_0. The cohesive edge is first determined by numerically solving (6), followed by solving for U_E, U_S, and U_T as functions of c. Figures 4a to 4c show the energy terms for $w_0 = 0.5$ and a range of p. At large p (>100), all energy terms approach the JKR limit. In Fig. 3c, the local minimum indicates a stable equilibrium. Figures 5a to 5c show $U_T(c)$ for fixed p and a range of w_0. In

Downloaded At: 19:39 21 January 2011

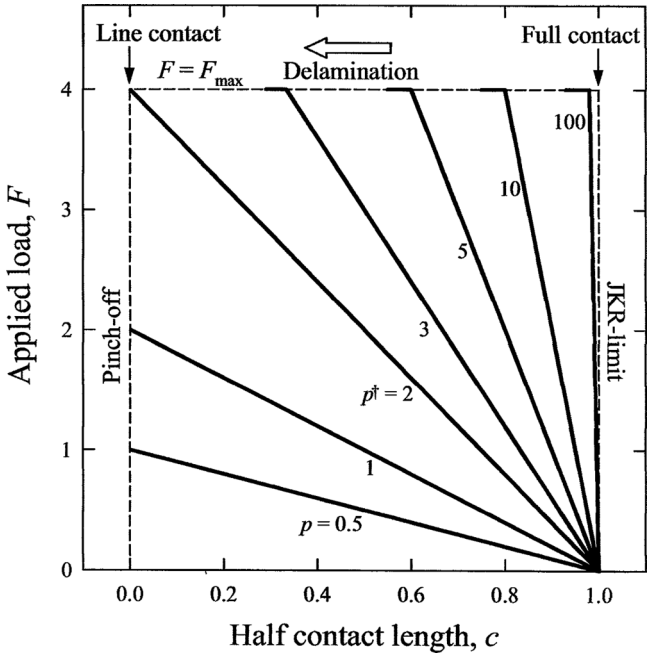

FIGURE 6 Applied load as a function of half contact length for a range of disjoining pressure. The curve with $p = p^\dagger = 2$ reaches a maximum load at pinch-off ($c = 0$).

Downloaded At: 19:39 21 January 2011

Fig. 4a, $p = 0.5$ and the DMT limit applies throughout. As the punch moves from $w_0 = 0$ to 0.1, the contact area decreases until pinch-off at w_0^*. Delamination proceeds along the dashed curve connecting the U_T minima from left to right. In Fig. 5b, $p = 5$ and $y = 0.2$. the DMT limit is valid for $w_0 \leq 0.2$. Further punch displacement leads to the DMT-JKR transition and the cohesive zone becomes fully developed. Figure 5c shows the JKR limit.

The full mechanical response, $F(w_0)$, for a range of p is shown in Fig. 3. For $p \leq p^\dagger$, the DMT limit is expected. All such curves ($p = 0.1$, 1, and 2) terminate at the locus OABC with $F^* = 16(w_0^*)^3$. For $p > p^\dagger$, all curves begin with the DMT limit prior to the DMT-JKR transition at $w_0 = y$. For instance, when $p = 4$, DMT is valid until $w_0 = \gamma/p = 0.25$ at R. In a load-controlled measurement, pull-off occurs at R since further increase in load is no longer confined to this energy balance curve. In a displacement-controlled measurement, further increase in w_0 is possible beyond R. Along RR′, the contact area reduces while external load remains constant at $F = 4$. The energy

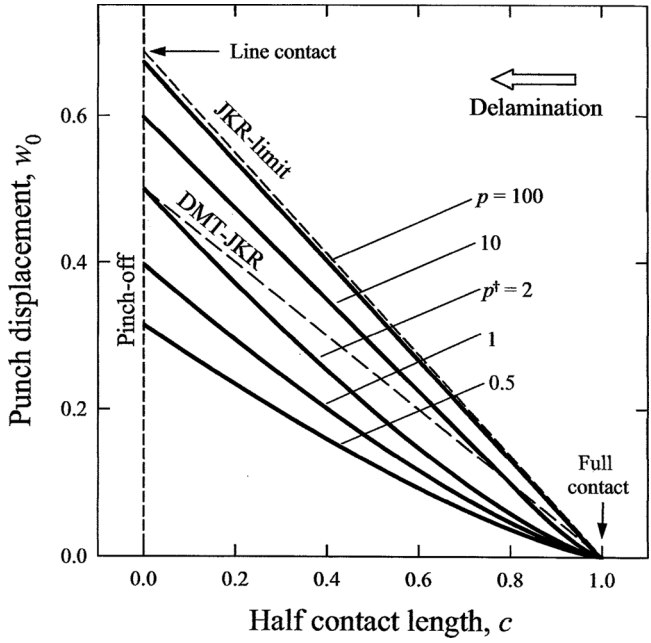

FIGURE 7 Punch displacement as a function of half contact length for a range of disjoining pressure. The dashed curve DMT-JKR indicates the transitional behavior. The curve with $p = p^{\dagger} = 2$ intersects the DMT-JKR line at $c = 0$.

Downloaded At: 19:39 21 January 2011

balance allows one to obtain the last loading point at R′, where $c = 0$ and the membrane pinches off the substrate. In the JKR limit, the loading curve rises sharply in F until $F = 4$ at J. Further increase in w_0 reduces contact area while F remains at 4 until pinch-off at J′. The same DMT-JKR transition is predicted for $p = 10$ along path OPP′. Useful expressions for $F(c)$ and $w_0(c)$ are shown in Figs. 6 and 7, respectively. In Fig. 6, delamination proceeds from bottom right ($c = 1$ and $F = 0$) to the left ($c = 0$). For $p > p^{\dagger}$, the external load staffs constant at F_{max} with decreasing contact area. The curves terminate at $c = 0$. In Fig. 7, the DMT limit is sufficient for $w_0 \leq y$. For $w_0 > y$, DMT-JKR transition occurs and the curve becomes linear until pinch-off at $c = 0$. The dashed line annotated "DMT-JKR" is the locus of the DMT-JKR transition and is found to be $w_0 = (1 - c)/2$. Figure 8 shows the varying cohesive edge as a function of half contact length. For $p \leq p^{\dagger}$, the DMT limit is valid and the cohesive zone extends to the membrane edge ($b = 1$). For $p > p^{\dagger}$, the trajectory deviates from the DMT limit at F_{max} and b decreases until pinch-off.

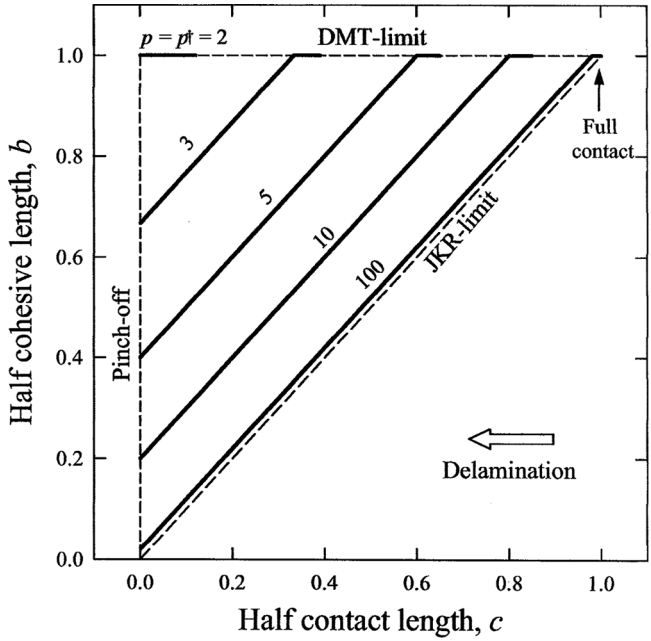

FIGURE 8 Cohesive edge as a function of half contact length for a range of disjoining pressure. Delamination proceeds from right to left. All curves initiate at $c = 1$ and $b = 1$ until deviation occurs at critical width.

Downloaded At: 19:39 21 January 2011

3. DISCUSSION

The above calculation leads to a slightly larger maximum force $F_{max} = 4$ compared with the classical JKR limit of $F_{max} = 3.884$ in our previous work [14] (*c.f.* Fig. 5). The 3% inconsistency lies in the average membrane stress approximation within and without the cohesive zone [*c.f.* Eqs. (7) and (10)] in computing the membrane profile and ultimately the energy balance. A proper method is to allow membrane stress to vary as a function of distance from the contact edge. However, discontinuity and non-differentiability will become inevitable at the cohesive edge, let alone an analytical solution. An exact numerical solution is beyond the scope of this paper. Nevertheless, the small discrepancy does not change the trend of the DMT-JKR transition when disjoining pressure approaches the JKR limit. The JKR limit is, therefore, stated to be $F = 4$ instead of 3.884 in Fig. 5.

It is worthwhile to contrast the 1-D model with a 2-D axisymmetric membrane. We earlier derived a model for a circular membrane clamped at the periphery with a radius a_c and adhered to a circular

punch of the same radius, reminiscent of the current rectangular geometry [17]. To make a meaningful comparison, we choose to equate the normalized applied load. In 1-D, the membrane is here taken to be a square with the same width and length, and the normalized applied load is redefined to be $F = \boldsymbol{F}[12(1-\nu^2)\boldsymbol{a}^2/\boldsymbol{Eh}^4] = \boldsymbol{F}[6(1-\nu^2)\boldsymbol{a}_c^2/\pi\boldsymbol{Eh}^4]$, implying comparable characteristic length scale, $\boldsymbol{a}_c = (2\pi)^{1/2}\boldsymbol{a}$. Considering a membrane-substrate interface with a specific interfacial disjoining pressure, $\boldsymbol{p}$, the normalized quantities are given by $p_{1D} = \boldsymbol{p}[12(1-\nu^2)\boldsymbol{a}^2/\boldsymbol{Eh}^4]$ and $p_{2D} = \boldsymbol{p}[6(1-\nu)\boldsymbol{a}_c^4/\boldsymbol{Eh}^4] = 2\pi^2 p_{1D} \approx 20p_{1D}$, ignoring the effect due to Poisson's ratio. As an illustration, Fig. 9 compares the 1-D and 2-D mechanical responses. In the DMT limit ($p_{1D} = 0.05$ and $p_{2D} = 1$), delamination in both 1-D (path OA) and 2-D (path OB) is accompanied by a monotoniably increasing applied load until "pinch-off". The DMT-JKR transition ($p_{1D} = 5$ and $p_{2D} = 100$) shows contrasting 1-D (path OPP′) and 2-D (path OQQ′) behavior. The circular membrane reaches a maximum prior to the transition and decreases monotonically until "pull-off" occurs at a

Downloaded At: 19:39 21 January 2011

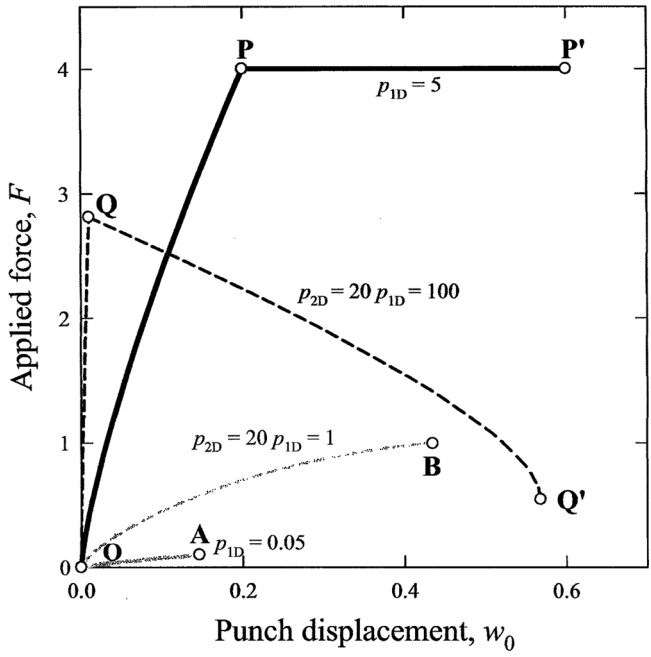

FIGURE 9 Comparison of mechanical response, $F(w_0)$, between 1-D model (solid) and the 2-D axisymmetric membrane clamped at the periphery (dashed). Pull-off occurs at Q′ and pinch-off at A, B, and P′.

non-zero radius. It is obvious that a gradual 1-D pinch-off causes less damage than an unstable 2-D pull-off. An ideal elliptical membrane delamination will follow an intermediate path bounded by the 1-D and 2-D limits.

The new model has significant impacts on the design of a number of cell-tissue adhesion, micro-devices, and micro-/nano-structures. For instance, we showed earlier that the stability of a micro-truss structure depends on combination of the bridge span, separation, and materials properties of the trusses, as well as the adhesion energy [16]. The finite magnitude and range of intersurface forces add a new dimension to the stability consideration and require new design guidelines.

4. CONCLUSION

The adhesion-delamination mechanics of a rectangular thin membrane is obtained by linear elasticity and thermodynamic energy balance. Pinch-off with a line contact and the associated critical force and central displacement are determined. The theoretical framework allows one to experimentally gauge the material properties of thin membranes and interfaces and to track the delamination process.

Downloaded At: 19:39 21 January 2011

ACKNOWLEDGMENTS

This work is supported by the National Science Foundation Grant CMMI # 0757140. Any opinions, findings, and conclusions or recommendations expressed in this material are those of the authors and do not necessarily reflect the views of the National Science Foundation. We are grateful to the reviewers for invaluable comments.

REFERENCES

[1] Zavracky, P. M., Majumder, S., and McGruer, N. E., *J. Microelectromech. S.* **6**, 3–9 (1997).
[2] Huang, W., Anvari, B., Torres, J. H., LeBaron, R. G., and Athanasiou, K. A., *J. Orthopaed. Res.* **21**, 88–95 (2003).
[3] Hertz, H., in *Miscellaneous Papers by H. Hertz*, D. E. Jones and G. A. Schott (Eds.) (Macmillian, London, 1896).
[4] Derjaguin, B. V., *Kolloid Z.* **69**, 155–164 (1934).
[5] Derjaguin, B. V., Muller, V. M., and Toporov, Y. P., *J. Colloid Interf. Sci.* **53** (2), 314–326 (1975).
[6] Johnson, K. L., Kendall, K., and Roberts, A. D., *P. Roy. Soc. A* **324**, 301–313 (1971).
[7] Maugis, D., *J. Colloid Interf. Sci.* **150**, 243–269 (1992).
[8] Foo, J. J., Chan, V., and Liu, K. K., *Ann. Biomed. Eng.* **31**, 1279–1286 (2003).
[9] Duan, G. and Wan, K.-T., *J. Appl. Mech.* **74**, 927–934 (2007).

[10] Majidi, C., Groff, R. E., and Fearing, R. S., *Math. Mech. Solids* **13**, 3–12, DOI: 10.1177/1081286506068823 (2008).
[11] Tang, T., Jogota, A., and Hui, C.-Y., *J. Appl. Phys.* **97**, DOI: 074304 (2005).
[12] Springman, R. M. and Bassani, J. L., *J. Mech. Phys. Solids* **57**, 909–931 (2009).
[13] Wan, K.-T., *J. Appl. Mech.* **69**, 110–116 (2002).
[14] Wan, K.-T. and Duan, J., *J. Appl. Mech.* **69**, 104–109 (2002).
[15] Wong, M.-F., Duan, G., and Wan, K.-T., *J. Adhesion* **83**, 67–83 (2007).
[16] Wong, M.-F., Duan, G., and Wan, K.-T., *J. Appl. Phys.* **101** (2), 024903 (2007).
[17] Wan, K.-T. and Julien, S. E., *J. Appl. Mech.* **76**, 051005 DOI: 10.1115/1.3112745 (2009).
[18] Wang, S. J. and Li, X., *Thin Solid Films* **515** (18), 7227–7231 (2007).
[19] Israelachvili, J. N., *Intermolecular and Surface Forces*, 3rd Edition, (Academic Press, London, 2010).
[20] Maugis, D., *Contact, Adhesion and Rupture of Elastic Solids*, (Springer, New York, 2000).
[21] Wan, K.-T. and Lawn, B. R., *Acta Metall. Mater.* **40** (2), 3331–3337 (1992).
[22] Barenblatt, G. I., *Adv. Appl. Mech.* **7**, 55–129 (1962).
[23] Lawn, B. R., in *Fracture of Brittle Solids*, Cambridge Solid State Science Series, E. A. Davis and I. M. Ward (Eds.) (Cambridge University Press, Cambridge, 1993).

Downloaded At: 19:39 21 January 2011